

Transport and localization properties of excitations in one-dimensional lattices with diagonal disordered mosaic modulations

Ba Phi Nguyen*

*Department of Basic Sciences, MienTrung University of Civil Engineering, Tuy Hoa 620000, Vietnam and
Research Institute for Basic Sciences, Ajou University, Suwon 16499, Korea*

Kihong Kim†

*Department of Physics, Ajou University, Suwon 16499, Korea and
School of Physics, Korea Institute for Advanced Study, Seoul 02455, Korea*

We present a numerical study of the transport and localization properties of excitations in one-dimensional lattices with diagonal disordered mosaic modulations. The model is characterized by the modulation period κ and the disorder strength W . We calculate the disorder averages $\langle T \rangle$, $\langle \ln T \rangle$, and $\langle P \rangle$, where T is the transmittance and P is the participation ratio, as a function of energy E and system size L , for different values of κ and W . For excitations at quasisonance energies determined by κ , we find power-law scaling behaviors of the form $\langle T \rangle \propto L^{-\gamma_a}$, $\langle \ln T \rangle \approx -\gamma_g \ln L$, and $\langle P \rangle \propto L^\beta$, as L increases to a large value. In the strong disorder limit, the exponents are seen to saturate at the values $\gamma_a \sim 0.5$, $\gamma_g \sim 1$, and $\beta \sim 0.3$, regardless of the quasisonance energy value. This behavior is in contrast to the exponential localization behavior occurring at all other energies. The appearance of sharp peaks in the participation ratio spectrum at quasisonance energies provides additional evidence for the existence of an anomalous power-law localization phenomenon. The corresponding eigenstates demonstrate multifractal behavior and exhibit unique node structures. In addition, we investigate the time-dependent wave packet dynamics and calculate the mean square displacement $\langle m^2(t) \rangle$, spatial probability distribution, participation number, and return probability. When the wave packet's initial momentum satisfies the quasisonance condition, we observe a subdiffusive spreading of the wave packet, characterized by $\langle m^2(t) \rangle \propto t^\eta$ where η is always less than 1. We also note the occurrence of partial localization at quasisonance energies, as indicated by the saturation of the participation number and a nonzero value for the return probability at long times.

I. INTRODUCTION

According to the scaling theory of Anderson localization in noninteracting systems, localization occurs in one- and two-dimensional systems with arbitrarily weak disorder, and in three-dimensional systems with strong enough disorder [1, 2]. Despite extensive studies on Anderson localization [3–8], there are still several aspects that are not fully understood, and new types of localization phenomena continue to be discovered [9–33]. Recent examples include unconventional transport in disordered quantum wires [9–13], localization in disordered non-Hermitian systems [14–20], and the quantum boomerang effect in both Hermitian and non-Hermitian systems [21–25].

It is well-known that in one-dimensional (1D) noninteracting systems with uncorrelated disorder, long-range transport is absent due to Anderson localization [3]. This can be observed through an exponential decrease in transmittance with thickness for extended excitations, and a saturation of mean-square displacement at long times for initially localized excitations. However, studies have shown that certain types of correlations in the disorder distribution can enable long-range transport. For example, the binary random dimer model exhibits a discrete set of resonance energies [34–38], where the mean-

square displacement grows as $t^{3/2}$ over time t , indicating superdiffusive transport behavior [36]. Additionally, the transmittance across the system is identically equal to 1 in the scattering problem. This superdiffusive behavior has been observed in optical experiments [38]. The binary random dimer model has been extended to the binary random N -mer model, and analytical expressions have been derived to identify the resonant energies that trigger delocalization [39, 40].

Our recent numerical investigation explored the time-dependent reflection of wave packets incident on an effectively semi-infinite disordered mosaic lattice chain, where disordered on-site potentials are inserted into the lattice only at equally spaced sites [41]. Through extensive numerical calculations, we discovered a discrete set of quasisonance energies that deviate sharply from the ordinary Anderson localization behavior. We derived a simple analytical formula for these energies, which interestingly takes the same form as the resonance energy formula found in the binary random N -mer model [39]. However, it is important to note that this similarity is purely coincidental, as the underlying mechanisms are entirely distinct [41]. The binary random N -mer model exhibits superdiffusive wave packet spreading and completely extended states at resonance energies. Therefore, a natural question arises: how do these phenomena change at the quasisonance energies present in the disordered mosaic lattice model? One of our primary goals is to address this question in the present study. It

* nguyebaphi@muce.edu.vn

† khkim@ajou.ac.kr

is worth noting that 1D mosaic lattice models of various types have yielded many interesting results in recent years [42–48].

In this paper, we aim to further expand our previous research and investigate the nature of states at quiresonance energies in more detail through calculations of several other physical quantities. Specifically, we study three different characteristics. First, we calculate the disorder averages of the transmittance and the logarithm of transmittance, denoted as $\langle T \rangle$ and $\langle \ln T \rangle$, in the scattering geometry and perform a finite-size scaling analysis of the results. Second, we calculate the averaged participation ratio $\langle P \rangle$ by solving the eigenvalue problem. For excitations at quiresonance energies, we find power-law scaling behaviors of the form $\langle T \rangle \propto L^{-\gamma_a}$, $\langle \ln T \rangle \approx -\gamma_g \ln L$, and $\langle P \rangle \propto L^\beta$, as the system length L increases to a large value. This behavior is in stark contrast to the exponential localization behavior displayed at all other energies. The appearance of sharp peaks in the participation ratio spectrum at quiresonance energies lends further support to the notion of an anomalous power-law localization effect. The corresponding eigenstates demonstrate multifractal behavior and exhibit unique node structures. Thirdly, we investigate the time-dependent wave packet dynamics and calculate the mean square displacement $\langle m^2(t) \rangle$, spatial probability distribution, participation number, and return probability. When the wave packet's initial momentum satisfies the quiresonance condition, we consistently observe a subdiffusive spreading of the wave packet, characterized by $\langle m^2(t) \rangle \propto t^\eta$ where $0 < \eta < 1$. Furthermore, we note the occurrence of partial localization at quiresonance energies, as indicated by the saturation of the participation number and a nonzero value for the return probability at long times.

The rest of this paper is organized as follows. In Sec. II, we introduce the 1D disordered mosaic lattice model. The results of the numerical calculations are presented in the order of wave transmittance, participation ratio, and time-dependent wave packet dynamics in Sec. III. Finally, we conclude the paper in Sec. IV.

II. MODEL

We consider a quantum particle that moves along a 1D lattice, which can be characterized by the time-dependent discrete Schrödinger equation

$$i\hbar \frac{dC_n}{dt} = V_n C_n + J(C_{n-1} + C_{n+1}), \quad (1)$$

where $C_n(t)$ is the probability amplitude of finding the particle at the n -th site, subject to the normalization condition $\sum_n |C_n(t)|^2 = 1$. V_n is the on-site potential at the n -th site and J is the coupling strength between adjacent sites. From now on, we measure all energy scales in the units of J and set $J = \hbar = 1$, which implies that the energy coincides with the frequency. The stationary

solutions of Eq. (1) can be represented in the conventional form, $C_n(t) = \psi_n e^{-iEt}$, where E is the energy of an eigenstate. Then we obtain

$$E\psi_n = V_n \psi_n + \psi_{n-1} + \psi_{n+1}. \quad (2)$$

In the present study, we will investigate the transport and localization properties of a disordered mosaic lattice model characterized by an on-site potential of the following form:

$$V_n = \begin{cases} \varepsilon_n \in [-W, W], & n = m\kappa \\ V_0, & \text{otherwise} \end{cases}, \quad (3)$$

where κ is a positive integer referred to as the mosaic modulation period and m is an integer ranging from 1 to N . This equation specifies that the on-site potential undergoes mosaic modulation with a periodicity of κ . The total number of sites L is equal to κN . The on-site potential ε_n at the $m\kappa$ -th site is a uniformly distributed random variable over the interval $[-W, W]$, where W represents the magnitude of disorder. At all the other sites, the on-site potential remains constant with a value of V_0 . The disordered mosaic lattice model has been the subject of recent investigation, with emphasis on numerical analysis of the time-dependent reflectance of wave packets incident upon a lattice with a large length L [41]. The current study significantly expands on previous research by exploring additional aspects of the transport and localization properties of the same model, within the context of both stationary and non-stationary problems.

III. NUMERICAL RESULTS

In this section, we provide comprehensive numerical results in the order of wave transmittance, participation ratio, and time-dependent wave packet dynamics.

A. Wave transmittance

We assume that a plane wave is incident from the right side of a 1D lattice chain of length L and define the amplitudes of the incident, reflected, and transmitted waves, r_0 , r_1 , and t , by

$$\psi_n = \begin{cases} r_0 e^{-iq(n-L)} + r_1 e^{iq(n-L)}, & n \geq L \\ t e^{-iqn}, & n \leq 0 \end{cases}, \quad (4)$$

where the wave number q is related to E by the free-space dispersion relation $E = 2 \cos q$. In the absence of dissipation, the conservation law $|r_1|^2 + |t|^2 = |r_0|^2$ is satisfied. We choose the overall constant phase for the wave functions such that t corresponds to a positive real number.

The transmission coefficient is a crucial parameter for determining the nature of the states, and in experiments, it is associated with the dc conductivity of the system being studied. In order to compute the transmittance

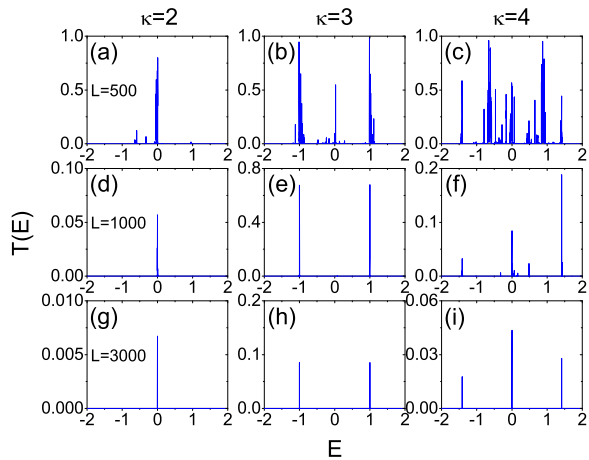


FIG. 1. Transmittance T plotted versus energy E when $\kappa = 2, 3, 4$, $L = 500, 1000, 3000$, $W = 1$, and $V_0 = 0$ for a single disorder configuration. When L is sufficiently large ($L = 3000$), T remains non-negligible only at the $(\kappa - 1)$ special energy values, such as $E = 0$ for $\kappa = 2$, $E = \pm 1$ for $\kappa = 3$, and $E = 0, \pm\sqrt{2}$ for $\kappa = 4$.

and reflectance numerically, we begin by selecting a positive real number for t arbitrarily. Then we use the relationships $\psi_{-1} = te^{iq}$, $\psi_0 = t$, and $\psi_1 = E\psi_0 - \psi_{-1}$ and solve Eq. (2) iteratively until we obtain ψ_L and ψ_{L+1} . Next, using the relationships $\psi_L = r_0 + r_1$ and $\psi_{L+1} = r_0e^{-iq} + r_1e^{iq}$, we compute

$$r_0 = \frac{\psi_L e^{iq} - \psi_{L+1}}{e^{iq} - e^{-iq}}, \quad r_1 = \frac{-\psi_L e^{-iq} + \psi_{L+1}}{e^{iq} - e^{-iq}}. \quad (5)$$

Finally, the transmittance T and the reflectance R are obtained from

$$T(E) = \left| \frac{t}{r_0} \right|^2 = |t|^2 \frac{4 \sin^2 q}{|\psi_L e^{iq} - \psi_{L+1}|^2}, \quad (6)$$

$$R(E) = \left| \frac{r_1}{r_0} \right|^2 = \left| \frac{\psi_L e^{-iq} - \psi_{L+1}}{\psi_L e^{iq} - \psi_{L+1}} \right|^2. \quad (7)$$

In the $\kappa = 1$ case corresponding to the ordinary Anderson model, the transmittance decreases exponentially with L and vanishes in the $L \rightarrow \infty$ limit for all states [4, 5]. When the mosaic modulation is turned on, however, the behavior changes substantially. In Fig. 1, we plot the transmittance T as a function of E when $\kappa = 2, 3, 4$ and $L = 500, 1000, 3000$ for a single disorder configuration. The parameters W and V_0 are fixed to $W = 1$ and $V_0 = 0$. When L is small, T is substantially large for many different E values as shown in Figs. 1(a), 1(b), and 1(c). However, when L is sufficiently large (e.g., $L = 3000$), we find that T remains non-negligible only at the $(\kappa - 1)$ special energy values, such as $E = 0$ for $\kappa = 2$, $E = \pm 1$ for $\kappa = 3$, and $E = 0, \pm\sqrt{2}$ for $\kappa = 4$, as shown in Figs. 1(g), 1(h), and 1(i). At these energies, the transmittance decays much more slowly than at other values of E

where it decays exponentially with L . Recently, we have investigated the characteristics of these spectral points, primarily by analyzing the time-dependent reflectance of the incident wave packet through numerical calculations. [41]. We have demonstrated that in the long-time limit, almost all the incident wave packets exhibit the exponential localization behavior, whereas those at a discrete set of the $(\kappa - 1)$ energy values given by

$$E_R = V_0 + 2 \cos\left(\frac{\pi n}{\kappa}\right) \quad (n = 1, 2, \dots, \kappa - 1) \quad (8)$$

behave distinctly. We have shown that this is a kind of quairesonance phenomenon rather than a true resonance and the transmittance at E_R is always less than 1.

In order to get a more detailed understanding of the transmission properties at the quairesonance energies, we perform a finite-size scaling analysis of the disorder-averaged quantities $\langle \ln T \rangle$ and $\langle T \rangle$. In the Anderson localized regime, it is expected that $\langle \ln T \rangle \approx -L/\xi_g$ and $\langle T \rangle \propto e^{-L/\xi_a}$ as $L \rightarrow \infty$, where the quantity ξ_g is conventionally defined to be the localization length. At the quairesonance energies, however, markedly different behaviors are obtained. In Fig. 2, we plot $\langle \ln T \rangle$ and $\langle T \rangle$ versus L at three quairesonance energies $E = 0$ for $\kappa = 2$, $E = 1$ for $\kappa = 3$, and $E = \sqrt{2}$ for $\kappa = 4$, when $W = 1, 2, 3$ and $V_0 = 0$. The disorder averaging is done over 50000 independent disorder configurations. In the insets in the upper-right corners, it is shown that $\langle \ln T \rangle \approx -\gamma_g \ln L$ and $\langle T \rangle \propto L^{-\gamma_a}$ in the large- L region. The power-law exponents γ_a and γ_g saturate at the values $\gamma_a \sim 0.5$ and $\gamma_g \sim 1$ when $W \rightarrow \infty$. When the energy is slightly different from the quairesonance values, the exponential localization behavior such that $\langle \ln T \rangle \propto -L/\xi_g$ is shown to be recovered.

A similar power-law-type behavior of $\langle \ln T \rangle$ and $\langle T \rangle$ occurs in other random systems, which include 1D disordered systems in an external electric (or bias) field and some random models with Kerr-type nonlinearity [31, 49–52]. This behavior is often referred to as anomalous localization. The power-law exponents γ_a and γ_g are determined by a numerical fitting of the data. It has been argued that the exponent γ_g is substantially larger than γ_a due to large fluctuation effects associated with the statistical distribution [31]. In order to show that the anomalous localization behavior occurs only at the quairesonance energies, we plot $\langle \ln T \rangle$ versus L for some values of E that deviate only slightly from the quairesonance energies, in the insets of Figs. 2(a), 2(c), and 2(e). In all the cases presented, the transmittance clearly exhibits an exponential decay with L , indicating the standard localization behavior. We have also verified numerically that this behavior occurs for all values of E that are not very close to the quairesonance energies.

In Fig. 3, we show examples of the spatial distribution of wave function intensity at certain quairesonance energies for a specific disorder realization, when the system size L is 3000 and a plane wave is incident from the region where $L > 3000$. The wave function intensity is normalized by that of the incident wave, $|r_0|^2$. We observe that,

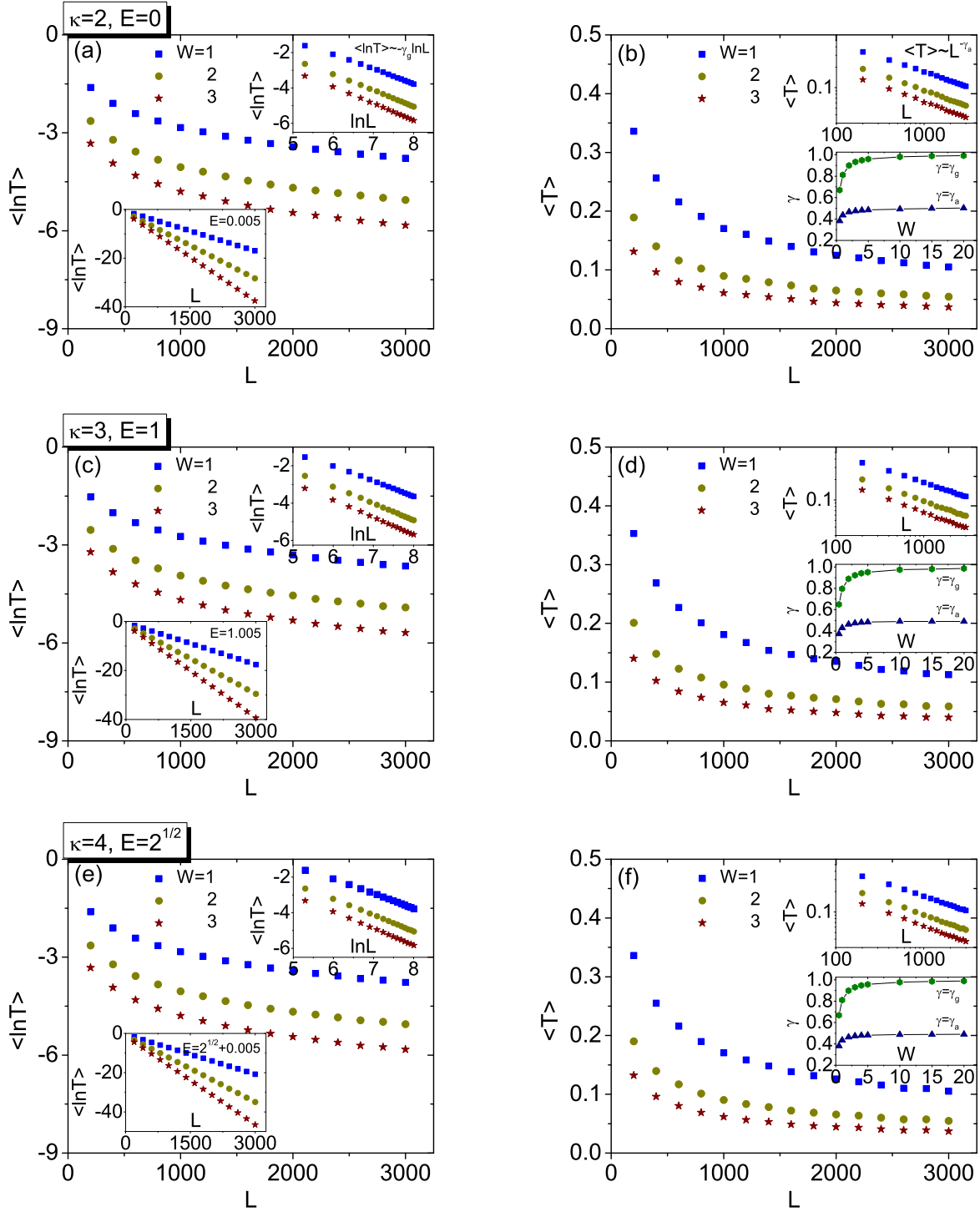


FIG. 2. Disorder-averaged quantities $\langle \ln T \rangle$ and $\langle T \rangle$ plotted versus L at the quasiresonance energies (a,b) $E = 0$ for $\kappa = 2$, (c,d) $E = 1$ for $\kappa = 3$, and (e,f) $E = \sqrt{2}$ for $\kappa = 4$, when $W = 1, 2, 3$ and $V_0 = 0$. In the insets in the upper-right corners, it is shown that $\langle \ln T \rangle \approx -\gamma_g \ln L$ and $\langle T \rangle \propto L^{-\gamma_a}$ in the large- L region. The power-law exponents γ_a and γ_g saturate at the values $\gamma_a \sim 0.5$ and $\gamma_g \sim 1$ when $W \rightarrow \infty$, as shown in the lower insets in the right-hand panels. When the energy is slightly different from the quasiresonance values, the exponential localization behavior such that $\langle \ln T \rangle \propto -L$ is recovered as shown in the lower insets in the left-hand panels.

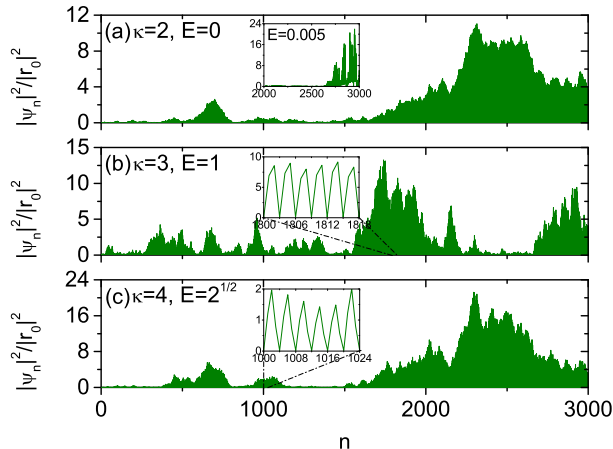


FIG. 3. Spatial distribution of the intensity of the wave function normalized by that of the incident wave for one particular realization of the random potential, when a plane wave is incident from the right side. Quasiresonance energies (a) $E = 0$ for $\kappa = 2$, (b) $E = 1$ for $\kappa = 3$, and (c) $E = \sqrt{2}$ for $\kappa = 4$ are considered. In the inset of (a), an example of a localized wave function at a slightly different energy is shown for the comparison with the quasiresonant case. In the insets of (b) and (c), it is shown that the wave functions at the quasiresonance energies have a node structure such that they vanish at all the sites $n = m\kappa$ for any integer m .

despite extending across almost the entire system, the wave function displays significant fluctuations in its envelope at quasiresonance energies. This indicates that the associated states are not entirely extended or exponentially localized. Instead, the wave function appears as multiple disconnected patches, a unique feature commonly seen in multifractal or critical states [53]. This is in contrast to the wave function corresponding to ordinary localization, as shown in the inset of Fig. 3(a). In Ref. 41, we have given an argument that at the quasiresonance energies, the wave function should exhibit a node structure where it is zero at all the lattice sites $m\kappa$ for any integer m , as demonstrated in the insets of Figs. 3(b) and 3(c). A similar intrinsic node structure of the wave function is observed to occur at all the other quasiresonance energies. This is a crucial feature that connects the periodic and disordered mosaic lattice models and gives rise to the critical states at the quasiresonance energies.

B. Participation ratio

In this subsection, we examine the eigenvalue problem for the stationary discrete Schrödinger equation given by Eq. (2). We numerically solve the eigenvalue problem of the form

$$\mathcal{H}\Psi = E\Psi \quad (9)$$

to obtain the eigenvalues E and the corresponding eigenfunctions $\Psi = (\psi_1, \psi_2, \dots, \psi_L)^T$. Using the open boundary condition, $\psi_0 = \psi_{L+1} = 0$, the matrix representation of \mathcal{H} is given by

$$\mathcal{H} = \begin{pmatrix} V_1 & 1 & 0 & \cdots & 0 & 0 \\ 1 & V_2 & 1 & \cdots & 0 & 0 \\ 0 & 1 & V_3 & \cdots & 0 & 0 \\ \vdots & \vdots & \vdots & \cdots & \vdots & \vdots \\ 0 & 0 & 0 & \cdots & 1 & V_L \end{pmatrix}. \quad (10)$$

In order to estimate the degree of spatial extension or localization of the eigenstates in disordered systems, we calculate the participation ratio P . For the k -th eigenstate $(\psi_1^{(k)}, \psi_2^{(k)}, \dots, \psi_L^{(k)})^T$ with the corresponding eigenvalue E_k , the participation ratio $P(E_k)$ is defined by

$$P(E_k) = \frac{\left(\sum_{n=1}^L |\psi_n^{(k)}|^2\right)^2}{\sum_{n=1}^L |\psi_n^{(k)}|^4}. \quad (11)$$

For a finite system, the value of P gives approximately the number of sites over which the k -th eigenfunction is extended. It has been known that in the localized case, P is closely related to the localization length, ξ_g [54]. The participation ratio generally represents an upper bound for the localization length ($P \geq \xi_g$). When L is sufficiently large, one finds a power-law scaling behavior of the form

$$\langle P(E) \rangle \propto L^\beta \quad (12)$$

with the scaling exponent β . $\langle P(E) \rangle$ is a double-averaged quantity, where $P(E)$ is obtained by averaging over all eigenstates within a narrow interval ΔE ($= 0.1$) around E and $\langle \dots \rangle$ denotes averaging over a large number of independent random realizations. It is well-established that for extended states, $\langle P(E) \rangle$ increases linearly with L and the exponent β is equal to 1. In contrast, for exponentially localized states, β is zero and $\langle P(E) \rangle$ does not depend on L and converges to a constant value in the $L \rightarrow \infty$ limit. For critical states, the scaling exponent should be in the range of $0 < \beta < 1$. Therefore the finite-size scaling analysis of $\langle P(E) \rangle$ provides very useful information about the nature of the states.

In Fig. 4, we show $\langle P(E) \rangle$ obtained by averaging over 1000 distinct disorder realizations as a function of energy E when $\kappa = 2, 3, 4$, $W = 0.5, 1, 2$, $V_0 = 0$, and $L = 1000$. We find that $\langle P(E) \rangle$ is sharply enhanced at all the quasiresonance energy values E_R given by Eq. (8), which implies that the localization is strongly suppressed at such energies. These results are fully consistent with those obtained in the previous subsection. The sharp peak at $E = 0$ is expected to occur only when κ is even. However, if we pay close attention to the case of $\kappa = 3$, a relatively small peak at $E = 0$ is clearly seen when the disorder is sufficiently weak (e.g., $W = 0.5$) [see Fig. 4(b)]. This peak occurs due to the band-center

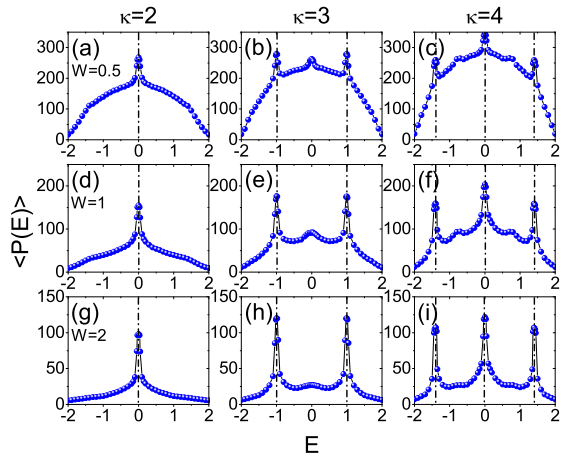


FIG. 4. Participation ratio averaged over 1000 distinct disorder configurations, $\langle P(E) \rangle$, plotted versus energy E when $\kappa = 2, 3, 4$, $W = 0.5, 1, 2$, $V_0 = 0$, and $L = 1000$. $\langle P(E) \rangle$ is sharply enhanced at the quasiresonance energy values $E = 0$ for $\kappa = 2$, $E = \pm 1$ for $\kappa = 3$, and $E = 0, \pm \sqrt{2}$ for $\kappa = 4$.

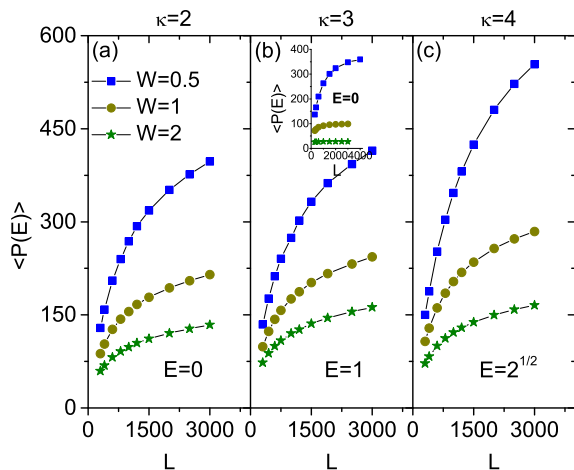


FIG. 5. Disorder-averaged participation ratio $\langle P(E) \rangle$ versus L at (a) $E = 0$ for $\kappa = 2$, (b) $E = 1$ for $\kappa = 3$, and (c) $E = \sqrt{2}$ for $\kappa = 4$, when $W = 0.5, 1, 2$ and $V_0 = 0$. In all the cases, $\langle P(E) \rangle$ scales as L^β with $0 < \beta < 1$ for sufficiently large L . The inset in (b) shows $\langle P(E) \rangle$ versus L when $E = 0$ and $\kappa = 3$.

anomaly (or Kappus-Wegner anomaly) and arises from the hidden symmetry at this spectral point [55–58]. One important difference between this peak and those at the quasiresonance energies will be pointed out below.

In order to understand the critical nature of the states at the quasiresonance energies, we perform a finite-size scaling analysis of $\langle P(E) \rangle$ based on the power-law ansatz, Eq. (12). In Fig. 5, we present the results of numerical calculations of $\langle P(E) \rangle$ versus L at $E = 0$ for $\kappa = 2$, $E = 1$ for $\kappa = 3$, and $E = \sqrt{2}$ for $\kappa = 4$, when $W = 0.5, 1, 2$ and

TABLE I. Dependence of the scaling exponent β at several quasiresonance energies on the disorder strength W . β decreases and then saturates as W increases.

W	β		
	$E = 0$ ($\kappa = 2$)	$E = 1$ ($\kappa = 3$)	$E = \sqrt{2}$ ($\kappa = 4$)
0.5	0.446 ± 0.025	0.445 ± 0.022	0.529 ± 0.027
1	0.356 ± 0.018	0.352 ± 0.016	0.385 ± 0.022
2	0.325 ± 0.013	0.317 ± 0.012	0.336 ± 0.015

$V_0 = 0$. In all the cases, $\langle P(E) \rangle$ is found to behave as a power law $\langle P(E) \rangle \propto L^\beta$ with $0 < \beta < 1$. The exponent β obtained by fitting the data is listed in Table I. These results indicate that the eigenstates at the quasiresonance energies are neither extended nor exponentially localized, but critical states. We find that β is a decreasing function of W and converges to a saturation value in the strong disorder regime. Our numerical results seem to suggest that the limiting value of β is approximately independent of the quasiresonance energy.

We have also performed a finite-size scaling analysis of $\langle P(E) \rangle$ at $E = 0$ for $\kappa = 3$, which corresponds to the band-center anomaly. The result shows that the exponent β approaches towards zero as $L \rightarrow \infty$ regardless of the disorder strength W [54]. This implies that although the participation ratio at the band center increases anomalously, the state at this spectral point is still exponentially localized and is fundamentally different from the quasiresonant states appearing at E_R .

C. Time-dependent wave packet dynamics

Up to this point, our emphasis has been on the stationary properties of excitations in the disordered mosaic lattice model. Here, we shift our focus to the dynamic characteristics and explore how initially localized wave packets propagate over time. Previous research has demonstrated that critical states typically lead to subdiffusive wave packet spreading in the long-time limit [59, 60]. While there are various types of initial wave packets that can be employed, including a single-site δ function wave packet, it is most suitable to use a Gaussian wave packet with a finite initial momentum, as defined by [61]

$$C_n(t=0) = A_\sigma \exp \left[-\frac{(n-n_0)^2}{4\sigma^2} + iq(n-n_0) \right] \quad (13)$$

where σ and n_0 are the spatial width and the initial position of the wave packet, respectively. A_σ is the normalization constant that has to be determined according to $\sum_n |C_n(t)|^2 = 1$. It is reminded that q is the wave number related to E by $E = 2 \cos q$. It is worth mentioning that the initial wave packet defined by Eq. (13) possesses a momentum distribution that is also a Gaussian, centered around q , and its momentum width is inversely

proportional to the spatial width σ . In order to ensure that the lattice chain's dynamic evolution is governed by a clearly defined energy E , it is essential to employ wave packets with a narrow momentum distribution. For this reason, the spatial width σ is selected to be adequately broad to satisfy the condition that $q\sigma \gg 1$ [21].

We solve numerically the time-dependent discrete Schrödinger equation, Eq. (1), to determine the time evolution of an initially localized wave packet given by Eq. (13). To characterize the wave packet's spatial spreading over time, we calculate dynamic quantities such as the mean-square displacement, spatial probability distribution, participation number, and return probability.

1. Mean-square displacement and spatial probability distribution

The first quantity we focus on is the mean-square displacement $m^2(t)$ defined by

$$m^2(t) = \sum_{n=1}^L (n - n_0)^2 |C_n(t)|^2, \quad (14)$$

which measures the difference between the wave packet's position at time t and its initial position [62]. The asymptotic spreading of the ensemble-averaged quantity $\langle m^2(t) \rangle$ can be fitted using a power-law ansatz

$$\langle m^2(t) \rangle \propto t^\eta, \quad (15)$$

where $\langle \dots \rangle$ denotes the averaging over independent realizations of the disorder. By analyzing the scaling exponent η , we can identify the various transport regimes, such as ballistic ($\eta = 2$), superdiffusive ($1 < \eta < 2$), diffusive ($\eta = 1$), subdiffusive ($0 < \eta < 1$), and localized ($\eta = 0$) regimes.

In order to prevent unwanted boundary effects in the numerical simulations, the system size L must be adequately large such that the wave function amplitude is insignificant at the edges for the longest time considered. Subsequently, the numerical calculations are conducted using a system size of $L = 40000$, the longest evolution time $t_{\max} = 10^4$, and a time step of $\Delta t = 0.1$. This choice guarantees that $|C_n(t_{\max})|^2 < 10^{-50}$ at the edges. In addition, we have chosen $\sigma = 20$ and $n_0 = L/2$ and the value of all calculated quantities is averaged over 50 independent disorder realizations.

In Fig. 6, we plot the time evolution of $\langle m^2(t) \rangle$ of an initially localized Gaussian wave packet for $\kappa = 2, 3$, and 4 at $E = 0$ and 1, when $W = 2$ and $V_0 = 0$. We find that when the wave packet is released with an initial velocity that does not satisfy the quiresonance condition, Eq. (8), the temporal growth of $\langle m^2(t) \rangle$ ceases completely in the long-time limit. This behavior is characterized by the scaling exponent $\eta = 0$ in Eq. (15), which indicates the usual Anderson localization. In contrast, when the initial velocity of the wave packet does satisfy the

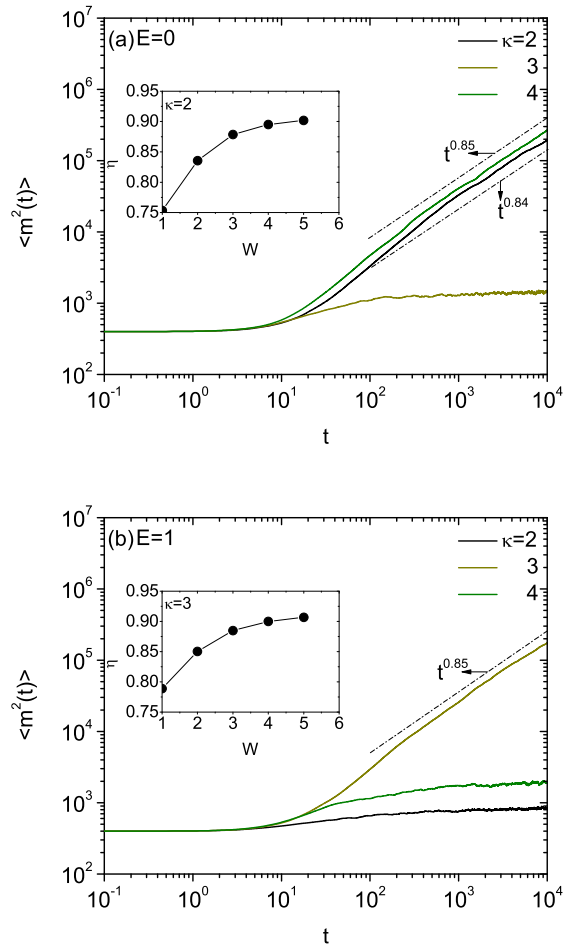


FIG. 6. Mean-square displacement obtained by averaging over 50 independent disorder realizations, $\langle m^2(t) \rangle$, plotted versus time t at (a) $E = 0$ and (b) $E = 1$, when $\kappa = 2, 3, 4$, $W = 2$, and $V_0 = 0$. All the results exhibit subdiffusive transport at the quiresonance energies such that $\langle m^2(t) \rangle \propto t^\eta$ with $0 < \eta < 1$. When the energy is not at the quiresonance energies, $\langle m^2(t) \rangle$ is seen to converge to a constant value and η approaches to 0. The W dependence of the scaling exponent η is shown in the insets.

quiresonance condition, a subdiffusive spreading with $0 < \eta < 1$ appears at long times. The exponent η has been determined by the fitting of the $\langle m^2(t) \rangle$ data in the range of $100 \leq t \leq 10^4$. When W is 2, we obtain $\eta \approx 0.835$ for $\kappa = 2$ and $\eta \approx 0.847$ for $\kappa = 4$ at $E = 0$ and $\eta \approx 0.851$ for $\kappa = 3$ at $E = 1$. The W dependence of η at these quiresonance energies is shown in the insets. We find that η is an increasing function of W , but its value is always less than 1, which indicates that the subdiffusive transport behavior observed at quiresonance energies remains robust. Like the other power-law exponents γ_a , γ_g , and β calculated in the previous subsections, we note that the exponent η approaches the same saturation value at all quiresonance energies as W increases.

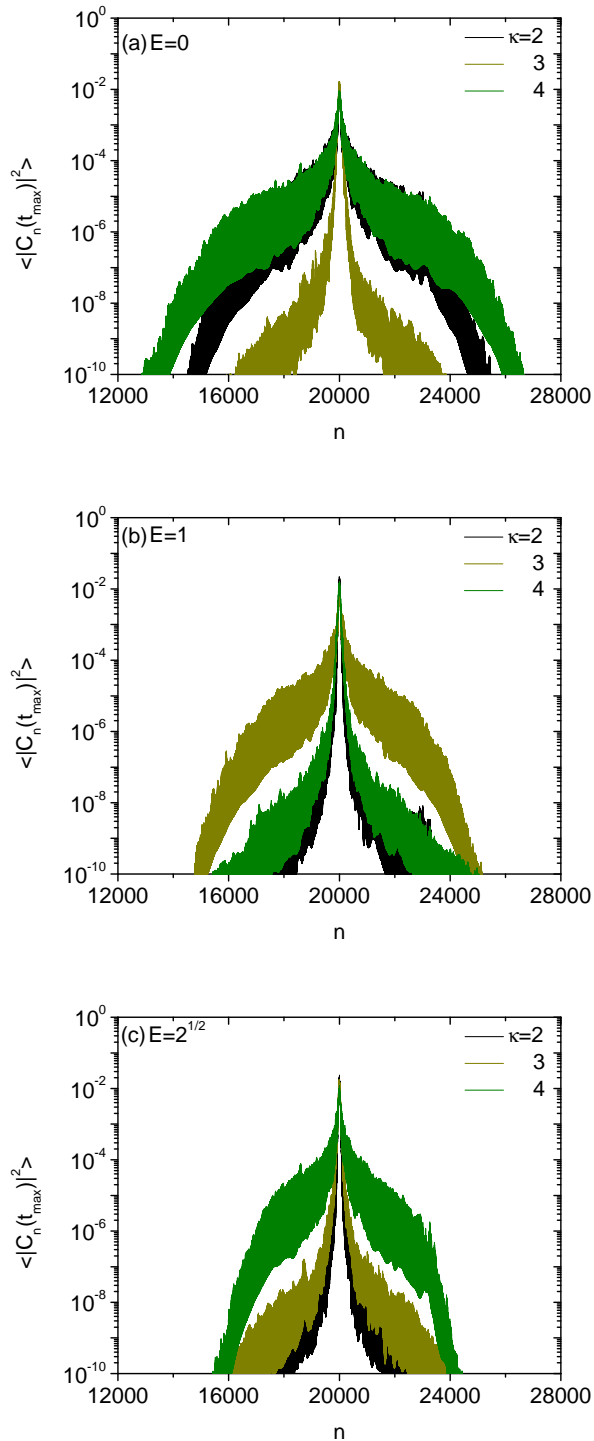


FIG. 7. Disorder-averaged probability distribution $\langle |C_n(t)|^2 \rangle$ versus site index n at $t = t_{\max} = 10^4$ when $\kappa = 2, 3, 4$, $W = 2$, $V_0 = 0$, and (a) $E = 0$, (b) $E = 1$, (c) $E = \sqrt{2}$. The values of $|C_n(t)|^2$ are averaged over the same 50 disorder realizations as in Fig. 6.

A more visual picture of the wave packet spreading over time can be obtained from plotting the averaged spatial probability distribution $\langle |C_n(t)|^2 \rangle$. In Fig. 7, we show $\langle |C_n(t)|^2 \rangle$ versus site index n at $t = t_{\max} = 10^4$ in a logarithmic plot. The other parameters are the same as in Fig. 6. Observations reveal three significant characteristics. The first feature involves the emergence of two distinct profiles for the averaged field distribution that are reliant on the localization behavior of the states. When the energy corresponds to quasiresonance energy, such as $E = 0$ for $\kappa = 2$ and 4, $E = 1$ for $\kappa = 3$, and $E = \sqrt{2}$ for $\kappa = 4$, the average field pattern displays a Gaussian-like characteristic profile and the logarithm of $\langle |C_n(t)|^2 \rangle$ decays parabolically away from the central region of the lattice. In contrast, when the energy does not correspond to quasiresonance energy, the average field pattern decays exponentially away from the central region of the lattice and the logarithm of $\langle |C_n(t)|^2 \rangle$ follows a linear curve, indicating the usual localization behavior. In previous studies of localization phenomena in nonlinear systems, similar characteristic field profiles have been observed experimentally in synthetic photonic lattices and ultracold-atom systems [63, 64]. The second feature is that when the quasiresonance condition is satisfied, the width of the wave packet gets broader when its initial velocity is larger. This is consistent with the calculated values of $\langle m^2(t) \rangle$ presented in Fig. 6. The third distinct feature is the emergence of a pronounced peak in the probability distribution at the center of the lattice, even when at quasiresonance energies. This indicates that while the edges of the wave packet undergo subdiffusive expansion within the lattice, its central part will remain localized near its original position for an extended period. This result will be further corroborated below.

2. Participation number and return probability

We now consider the participation number which gives an estimation of the number of lattice sites where the wave packet has a significant amplitude [62],

$$P_N(t) = \frac{1}{\sum_{n=1}^L |C_n(t)|^4}, \quad (16)$$

and the return probability defined by

$$R_0(t) = |C_{n_0}(t)|^2. \quad (17)$$

A quasiparticle is said to have escaped from its initial position when the return probability $R_0(t)$ vanishes in the long-time limit. In contrast, the value of $R_0(t \rightarrow \infty)$ remains finite for a localized wave packet. It has been known that the width of the spatial probability distribution of a wave packet is closely related to the mean-square displacement, while its amplitude is closely associated with the participation number and the return probability [60]. In Figs. 8 and 9, we show the disorder-averaged participation number $\langle P_N(t) \rangle$ and return probability $\langle R_0(t) \rangle$

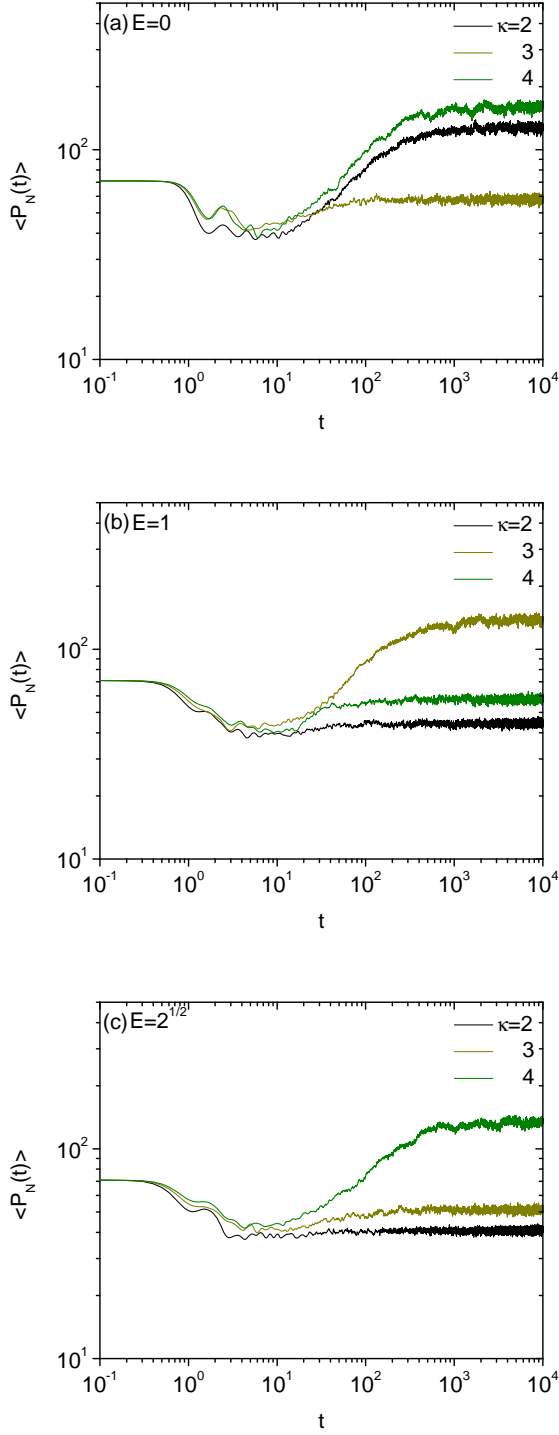


FIG. 8. Disorder-averaged participation number $\langle P_N(t) \rangle$ versus time t when $\kappa = 2, 3, 4$, $W = 2$, $V_0 = 0$, and (a) $E = 0$, (b) $E = 1$, (c) $E = \sqrt{2}$. $\langle P_N(t) \rangle$ reaches an asymptotically finite value at the quasi-resonance energies at which $\langle m^2(t) \rangle$ increases as a power law in time.

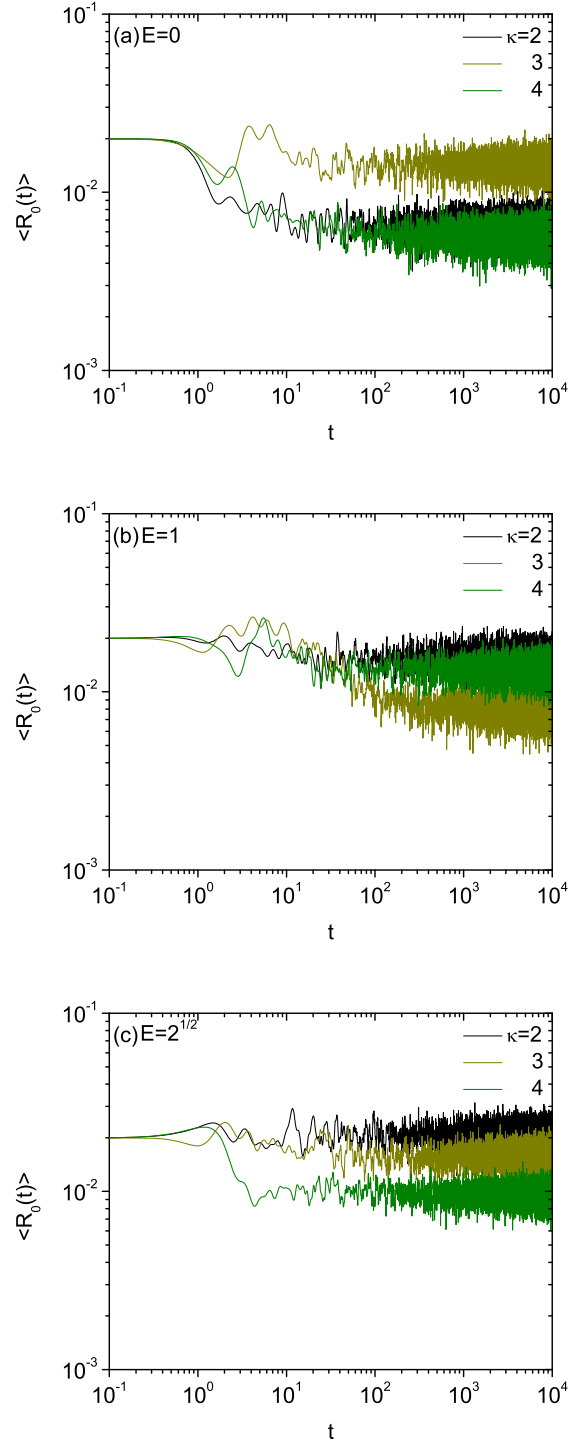


FIG. 9. Disorder-averaged return probability $\langle R_0(t) \rangle$ versus time t when $\kappa = 2, 3, 4$, $W = 2$, $V_0 = 0$, and (a) $E = 0$, (b) $E = 1$, (c) $E = \sqrt{2}$. It is observed that there is always a finite probability of finding the quasiparticle at the initial position as $t \rightarrow \infty$.

as a function of time t . All the numerical calculations are performed with the same parameters as in Fig. 6. The results show that a partial localization phenomenon occurs at all the quasisonance energies. A signature of the presence of partial localization is a saturation of $\langle P_N(t \rightarrow \infty) \rangle$ to a finite value as in the cases of $\kappa = 2$ and 4 in Fig. 8(a), though the corresponding values of $\langle m^2(t) \rangle$ keep increasing owing to the expanding edges as $t \rightarrow \infty$ as shown in Fig. 6(a). Similarly, asymptotically finite values of $\langle R_0(t \rightarrow \infty) \rangle$ are seen clearly in Fig. 9. The observed behavior is not limited to energies where regular Anderson localization takes place but is also evident at quasisonance energies, where subdiffusive transport is observed. All of these findings are in line with the existence of central peaks detected in the spatial probability distribution.

IV. CONCLUSION

In this paper, we have expanded our previous research on the disordered mosaic lattice model to perform detailed numerical calculations on various other physical quantities. Our earlier study focused on exploring the delocalization effect that arises at a finite number of quasisonance energies primarily by analyzing the behavior of time-dependent reflectance of incoming wave packets over a long time interval. In this study, we have examined the nature of states at quasisonance energies through calculations on the stationary quantities such as the disorder-averaged transmittance, logarithm of transmittance, and participation ratio, $\langle T \rangle$, $\langle \ln T \rangle$,

and $\langle P \rangle$, and the dynamic quantities such as the mean square displacement $\langle m^2(t) \rangle$, spatial probability distribution, participation number, and return probability. For excitations at quasisonance energies, we have found power-law scaling behaviors of the form $\langle T \rangle \propto L^{-\gamma_a}$, $\langle \ln T \rangle \approx -\gamma_g \ln L$, and $\langle P \rangle \propto L^\beta$. Furthermore, when the wave packet's initial momentum satisfies the quasisonance condition, we have observed a subdiffusive spreading of the wave packet, characterized by $\langle m^2(t) \rangle \propto t^\eta$ where η is always less than 1. We have also noted the occurrence of partial localization at quasisonance energies, as indicated by the saturation of the participation number and a nonzero value for the return probability at long times. The disordered mosaic lattice model studied in this paper can be readily realized experimentally using various physical systems, which include coupled optical waveguide arrays, synthetic photonic lattices, and ultracold atoms. We hope that the results presented here will be a useful contribution to the study of unconventional localization phenomena in disordered systems.

ACKNOWLEDGMENTS

This research was supported through a National Research Foundation of Korea Grant (NRF-2022R1F1A1074463) funded by the Korean Government. It was also supported by the Basic Science Research Program funded by the Ministry of Education (2021R1A6A1A10044950) and by the Global Frontier Program (2014M3A6B3063708).

-
- [1] E. Abrahams, P. W. Anderson, D. C. Licciardello, and T. V. Ramakrishnan, Scaling theory of localization: Absence of quantum diffusion in two dimensions, *Phys. Rev. Lett.* **42**, 673 (1979).
 - [2] P. A. Lee and T. V. Ramakrishnan, Disordered electronic systems, *Rev. Mod. Phys.* **57**, 287 (1985).
 - [3] P. W. Anderson, Absence of diffusion in certain random lattices, *Phys. Rev.* **109**, 1492 (1958).
 - [4] I. M. Lifshits, A. S. Gredeskul, and L. A. Pastur, *Introduction to the Theory of Disordered Systems* (Wiley, New York, 1988).
 - [5] P. Sheng, *Introduction to Wave Scattering, Localization and Mesoscopic Phenomena* (Academic Press, San Diego, 1995).
 - [6] F. Evers and A. D. Mirlin, Anderson transitions, *Rev. Mod. Phys.* **80**, 1355 (2008).
 - [7] A. Lagendijk, B. A. van Tiggelen, and D. Wiersma, Fifty years of Anderson localization, *Phys. Today* **62**, 24 (2009).
 - [8] F. M. Izrailev, A. A. Krokhin, and N. M. Makarov, Anomalous localization in low-dimensional systems with correlated disorder, *Phys. Rep.* **512**, 125 (2012).
 - [9] F. Falceto and V. A. Gopar, Conductance through quantum wires with Lévy-type disorder: Universal statistics in anomalous quantum transport, *Europhys. Lett.* **92**, 57014 (2010).
 - [10] I. Amanatidis, I. Klefogiannis, F. Falceto, and V. A. Gopar, Conductance of one-dimensional quantum wires with anomalous electron wave-function localization, *Phys. Rev. B* **85**, 235450 (2012).
 - [11] I. Amanatidis, I. Klefogiannis, F. Falceto, and V. A. Gopar, Coherent wave transmission in quasi-one-dimensional systems with Lévy disorder, *Phys. Rev. E* **96**, 062141 (2017).
 - [12] M. Saha, S. K. Maiti, and A. Purkayastha, Anomalous transport through algebraically localized states in one dimension, *Phys. Rev. B* **100**, 174201 (2019).
 - [13] L. A. Razo-López, A. Z. Genack, and V. A. Gopar, Statistics of coherent waves inside media with Lévy disorder, *Phys. Rev. Research* **3**, 023035 (2021).
 - [14] A. Basiri, Y. Bromberg, A. Yamilov, H. Cao, and T. Kottos, Light localization induced by a random imaginary refractive index, *Phys. Rev. A* **90**, 043815 (2014).
 - [15] B. P. Nguyen, D. K. Phung, and K. Kim, Anomalous localization enhancement in one-dimensional non-Hermitian disordered lattices, *J. Phys. A: Math. Theor.* **53**, 045003 (2020).

- [16] A. F. Tzortzakakis, K. G. Makris, A. Szameit, and E. N. Economou, Transport and spectral features in non-Hermitian open systems, *Phys. Rev. Research* **3**, 013208 (2021).
- [17] S. Weidemann, M. Kremer, S. Longhi, and A. Szameit, Coexistence of dynamical delocalization and spectral localization through stochastic dissipation, *Nat. Photonics* **15**, 576 (2021).
- [18] R. Wang, L. L. Zhang, and Z. Song, Anderson localization induced by complex potential, *J. Phys. Commun.* **5**, 095011 (2021).
- [19] B. P. Nguyen, T. K. T. Lieu, and K. Kim, Numerical study of the transverse localization of waves in one-dimensional lattices with randomly distributed gain and loss: effect of disorder correlations, *Waves Random Complex Media* **32**, 390 (2022).
- [20] S. Kim and K. Kim, Delocalization and re-entrant localization of flat-band states in non-Hermitian disordered lattice models with flat bands, *Prog. Theor. Exp. Phys.* **2023**, 013I01 (2023).
- [21] T. Prat, D. Delande, and N. Cherroret, Quantum boomerang-like effect of wave packets in random media, *Phys. Rev. A* **99**, 023629 (2019).
- [22] J. Janarek, D. Delande, N. Cherroret, and J. Zakrzewski, Quantum boomerang effect for interacting particles, *Phys. Rev. A* **102**, 013303 (2020).
- [23] L. Tessieri, Z. Akdeniz, N. Cherroret, D. Delande, and P. Vignolo, Quantum boomerang effect: Beyond the standard Anderson model, *Phys. Rev. A* **103**, 063316 (2021).
- [24] F. Noronha, J. A. S. Lourenço, and T. Macrì, Robust quantum boomerang effect in non-Hermitian systems, *Phys. Rev. B* **106**, 104310 (2022).
- [25] F. Noronha and T. Macrì, Ubiquity of the quantum boomerang effect in Hermitian Anderson-localized systems, *Phys. Rev. B* **106**, L060301 (2022).
- [26] D. Leykam, J. D. Bodyfelt, A. S. Desyatnikov, and S. Flach, Localization of weakly disordered flat band states, *Eur. Phys. J. B* **90**, 1 (2017).
- [27] K. Kim, Anderson localization of electromagnetic waves in randomly-stratified magnetodielectric media with uniform impedance, *Opt. Express* **23**, 14520 (2015).
- [28] K. Kim and S. Kim, Anderson localization and Brewster anomaly of electromagnetic waves in randomly-stratified anisotropic media, *Mater. Res. Express* **6**, 085803 (2019).
- [29] S. Kim and K. Kim, Anderson localization and delocalization of massless two-dimensional Dirac electrons in random one-dimensional scalar and vector potentials, *Phys. Rev. B* **99**, 014205 (2019).
- [30] S. Kim and K. Kim, Anderson localization of two-dimensional massless pseudospin-1 Dirac particles in a correlated random one-dimensional scalar potential, *Phys. Rev. B* **100**, 104201 (2019).
- [31] C. Crosnier de Bellaistre, A. Aspect, A. Georges, and L. Sanchez-Palencia, Effect of a bias field on disordered waveguides: Universal scaling of conductance and application to ultracold atoms, *Phys. Rev. B* **95**, 140201(R) (2017).
- [32] C. Crosnier de Bellaistre, C. Trefzger, A. Aspect, A. Georges, and L. Sanchez-Palencia, Expansion of a quantum wave packet in a one-dimensional disordered potential in the presence of a uniform bias force, *Phys. Rev. A* **97**, 013613 (2018).
- [33] G. Berthet, L. Lavoine, M. K. Parit, A. Brolis, A. Boissé, and T. Bourdel, Observation of the algebraic localization-delocalization transition in a one-dimensional disordered potential with a bias force, *Phys. Rev. Research* **2**, 013386 (2020).
- [34] D. H. Dunlap, H.-L. Wu, and P. W. Phillips, Absence of localization in a random-dimer model, *Phys. Rev. Lett.* **65**, 88 (1990).
- [35] H.-L. Wu, W. Goff, and P. Phillips, Insulator-metal transitions in random lattices containing symmetrical defects, *Phys. Rev. B* **45**, 1623 (1992).
- [36] P. K. Datta, D. Giri, and K. Kundu, Nonscattered states in a random-dimer model, *Phys. Rev. B* **47**, 10727 (1993).
- [37] F. M. Izrailev, T. Kottos, and G. P. Tsironis, Hamiltonian map approach to resonant states in paired correlated binary alloys, *Phys. Rev. B* **52**, 3274 (1995).
- [38] U. Naether, S. Stützer, R. A. Vicencio, M. I. Molina, A. Tünnermann, S. Nolte, T. Kottos, D. N. Christodoulides, and A. Szameit, Experimental observation of superdiffusive transport in random dimer lattices, *New J. Phys.* **15**, 013045 (2013).
- [39] A. Kosior, J. Major, M. Płodzień, and J. Zakrzewski, Role of correlations and off-diagonal terms in binary disordered one-dimensional systems, *Acta Phys. Pol.* **128**, 1002 (2015).
- [40] J. Major, Extended states in disordered one-dimensional systems in the presence of the generalized N -mer correlations, *Phys. Rev. A* **94**, 053613 (2016).
- [41] B. P. Nguyen, D. K. Phung, and K. Kim, Quasiresonant diffusion of wave packets in one-dimensional disordered mosaic lattices, *Phys. Rev. B* **106**, 134204 (2022).
- [42] Y. Wang, X. Xia, L. Zhang, H. Yao, S. Chen, J. You, Q. Zhou, and X.-J. Liu, One-dimensional quasiperiodic mosaic lattice with exact mobility edges, *Phys. Rev. Lett.* **125**, 196604 (2020).
- [43] Q.-B. Zeng and R. Lü, Topological phases and Anderson localization in off-diagonal mosaic lattices, *Phys. Rev. B* **104**, 064203 (2021).
- [44] Q.-B. Zeng, R. Lü, and L. You, Topological superconductors in one-dimensional mosaic lattices, *EPL* **135**, 17003 (2021).
- [45] Y. Liu, Y. Wang, X.-J. Liu, Q. Zhou, and S. Chen, Exact mobility edges, \mathcal{PT} -symmetry breaking, and skin effect in one-dimensional non-Hermitian quasicrystals, *Phys. Rev. B* **103**, 014203 (2021).
- [46] L.-Y. Gong, H. Lu, and W.-W. Cheng, Exact mobility edges in 1D mosaic lattices inlaid with slowly varying potentials, *Adv. Theory Simul.* **4**, 2100135 (2021).
- [47] D. Dwiputra and F. P. Zen, Single-particle mobility edge without disorder, *Phys. Rev. B* **105**, L081110 (2022).
- [48] Q.-B. Zeng and R. Lü, Real spectra and phase transition of skin effect in nonreciprocal systems, *Phys. Rev. B* **105**, 245407 (2022).
- [49] C. M. Soukoulis, J. V. José, E. N. Economou, and P. Sheng, Localization in one-dimensional disordered systems in the presence of an electric field, *Phys. Rev. Lett.* **50**, 764 (1983).
- [50] B. Doucot and R. Rammal, Invariant-embedding approach to localization. II. Non-linear random media, *J. Phys. (Paris)* **48**, 527 (1987).
- [51] Y. Sharabi, H. H. Sheinfux, Y. Sagi, G. Eisenstein, and M. Segev, Self-induced diffusion in disordered nonlinear photonic media, *Phys. Rev. Lett.* **121**, 233901 (2018).
- [52] A. Iomin, From power law to Anderson localization in nonlinear Schrödinger equation with nonlinear randomness, *Phys. Rev. E* **100**, 052123 (2019).

- [53] C. Castellani and L. Peliti, Multifractal wavefunction at the localisation threshold, *J. Phys. A: Math. Gen.* **19**, L429 (1986).
- [54] D. O. Krimer and S. Flach, Statistics of wave interactions in nonlinear disordered systems, *Phys. Rev. E* **82**, 046221 (2010).
- [55] M. Kappus and F. Wegner, Anomaly in the band centre of the one-dimensional Anderson model, *Z. Phys. B* **45**, 15 (1981).
- [56] L. I. Deych, M. V. Erementchouk, A. A. Lisyansky, and B. L. Altshuler, Scaling and the center-of-band anomaly in a one-dimensional Anderson model with diagonal disorder, *Phys. Rev. Lett.* **91**, 096601 (2003).
- [57] H. Schomerus and M. Titov, Band-center anomaly of the conductance distribution in one-dimensional Anderson localization, *Phys. Rev. B* **67**, 100201(R) (2003).
- [58] B. P. Nguyen and K. Kim, Anomalously suppressed localization in the two-channel Anderson model, *J. Phys.: Condens. Matter* **24**, 135303 (2012).
- [59] H. Hiramoto and S. Abe, Dynamics of an electron in quasiperiodic systems. II. Harper's model, *J. Phys. Soc. Jpn.* **57**, 1365 (1988).
- [60] M. Larcher, F. Dalfovo, and M. Modugno, Effects of interaction on the diffusion of atomic matter waves in one-dimensional quasiperiodic potentials, *Phys. Rev. A* **80**, 053606 (2009).
- [61] J. L. L. dos Santos, B. P. Nguyen, and F. A. B. F. de Moura, Electronic transport in disordered chains with saturable nonlinearity, *Physica A* **435**, 15 (2015).
- [62] M. Johansson, M. Hörnquist, and R. Riklund, Effects of nonlinearity on the time evolution of single-site localized states in periodic and aperiodic discrete systems, *Phys. Rev. B* **52**, 231 (1995).
- [63] T. Schwartz, G. Bartal, S. Fishman, and M. Segev, Transport and Anderson localization in disordered two-dimensional photonic lattices, *Nature* **446**, 52 (2007).
- [64] G. Roati, C. D'Errico, L. Fallani, M. Fattori, C. Fort, M. Zaccanti, G. Modugno, M. Modugno, and M. Inguscio, Anderson localization of a non-interacting Bose-Einstein condensate, *Nature* **453**, 895 (2008).